

# Topography of epitaxial GaAs surfaces for growth

S. Y. Lehman<sup>a)</sup>

*Department of Physics, The College of Wooster, Wooster, Ohio 44691*

A. Roshko,<sup>b)</sup> R. P. Mirin, K. A. Bertness, T. E. Harvey, and K. D. Cobry<sup>c)</sup>

*National Institute of Standards and Technology, Mailcode 815.04, 325 Broadway, Boulder, Colorado 80305-3328*

(Received 19 December 2008; accepted 23 March 2009; published 30 April 2009)

The topography and surface roughness of (100) GaAs substrates and buffers after different preparation procedures were determined from atomic force microscopy (AFM) measurements. In order to characterize the topography over a wide range of length scales, multiple large  $5 \times 5 \mu\text{m}^2$  AFM scans were acquired for each sample. These scans were analyzed both by histogramming the distribution of pixel heights and by finding the rms roughness at length scales from 10 nm to  $5 \mu\text{m}$  using a tiling analysis. The influence of substrate aging and chemical etching on buffers grown by molecular beam epitaxy was studied, as was the effect of different buffer growth procedures. Immediately after thermal desorption of the surface oxide, all wafers were extremely rough, as expected, with wafers etched in HCl:H<sub>2</sub>O (1:1) somewhat smoother than untreated epi-ready wafers, while wafers etched in H<sub>2</sub>O<sub>2</sub>:NH<sub>4</sub>OH:H<sub>2</sub>O (3:1:10) were rougher. After as little as 100 nm of buffer growth, however, there was no significant difference in roughness of etched or as-received substrates, and all samples were quite smooth with a rms roughness around 0.27 nm. The buffer growth conditions were found to significantly affect surface roughness. Interrupting the supply of Ga at the start of the growth enhanced mounding on the wafer surface, while postgrowth annealing at the growth temperature reduced the surface roughness and changed the characteristic topography of the surface. [DOI: 10.1116/1.3119684]

## I. INTRODUCTION

The topography of substrate surfaces plays a critical role in determining the success of epitaxial growth by molecular beam epitaxy (MBE) and organometallic vapor phase epitaxy (OMVPE). The smoothness of homoepitaxial films has generally been previously studied either directly at the atomic scale by scanning tunneling microscopy (STM)<sup>1-4</sup> or cross-sectional transmission electron microscopy<sup>5,6</sup> or indirectly at larger length scales by optical scattering<sup>7-10</sup> from the surface. Atomic force microscopy (AFM) has also been used to study topography at intermediate length scales,<sup>9,10</sup> typically with scan sizes less than  $1 \times 1 \mu\text{m}^2$ .

In this work, we have used AFM to characterize the surface topography over a much larger area, imaging each sample in multiple locations with large  $5 \times 5 \mu\text{m}^2$  scans. The AFM scans have been quantitatively analyzed with a novel technique to investigate the variation in surface roughness as a function of length scale. A bearing analysis was also used on these large-area scans to develop better techniques for distinguishing surface morphologies which appear different visually but have similar surface roughness.

We have applied these new topographical analysis techniques to homoepitaxial GaAs buffer layers grown by MBE on epi-ready samples with a variety of surface preparations and grown under several different growth conditions. We have previously observed different buffer layer morphologies

and characterized the effects of these differences on the formation of self-assembled quantum dots.<sup>11</sup> We describe here more fully the influence of both substrate preparation methods and buffer layer growth conditions on the roughness of GaAs buffer layers grown by MBE. Additionally, we identify growth conditions that lead to distinct buffer layer morphologies.

## II. EXPERIMENTAL METHODS

The substrates studied were 5 cm (2 in.) diameter, Si-doped,  $(100) \pm 0.1^\circ$  GaAs wafers. All wafers were sold as epi-ready (ready to be used for epitaxial growth without further chemical treatment) and were stored in their sealed epi-ready packages under ambient conditions for at least 1 year. Most substrates (with the exception of those used to grow samples AR-100, AR-500 R, and AR-500 AN2) were from the same boule and obtained at the same time from the manufacturer. Substrates with three different preparations were examined: (1) "as-received" wafers were used directly from their epi-ready packaging; (2) "HCl etched" wafers were etched in a 1:1 solution of HCl:H<sub>2</sub>O for 1 min at room temperature and rinsed under flowing de-ionized water; (3) "PAW-HCl etched" wafers were etched in a 3:1:10 solution of H<sub>2</sub>O<sub>2</sub>:NH<sub>4</sub>OH:H<sub>2</sub>O for 3 min at room temperature, rinsed under de-ionized water for 3 min, then dipped in a 1:1 solution of HCl:H<sub>2</sub>O and rinsed under de-ionized water. The wafers were quartered after the chemical treatment, mounted into indium-free wafer holders, and immediately loaded into the MBE system.

<sup>a)</sup>Electronic mail: slehman@wooster.edu

<sup>b)</sup>Electronic mail: roshko@boulder.nist.gov

<sup>c)</sup>Present address: University of Colorado, Boulder, Colorado 80309.

The beam equivalent pressures for both As and Ga were measured with a beam flux monitor that could be moved into the growth position such that the shield immediately behind the ion gauge was approximately 1 cm in front of the substrate. The As source was equipped with a cracking zone and variable orifice, so that most of the As flux is in the form of  $As_2$ . During this series of experiments, the Ga beam equivalent pressure for a growth rate of 1  $\mu\text{m}/\text{h}$  was between  $5.5 \times 10^{-5}$  and  $6.5 \times 10^{-5}$  Pa. Ga flux was measured without coevaporation of As, and typically readings required 1–2 min to stabilize. Because of variability in ion gauge sensitivity factors and As species, beam equivalent pressures are only an approximate guide to actual flux. Growth rates were determined from reflection high energy electron diffraction (RHEED) intensity oscillations, and in this growth regime where the Ga sticking coefficient is unity, the growth rate is the best indicator of Ga atomic flux.

Prior to buffer layer growth the surface oxide was removed by heating the substrates to 640 °C in the MBE chamber at a rate of 50 °C/min, with an As pressure of  $1.2 \times 10^{-3}$  Pa ( $9 \times 10^{-6}$  Torr). The oxide desorption was confirmed by RHEED and typically was complete around 625 °C. After being held at 640 °C for approximately 1 min the substrates were cooled to 600 °C. The substrate temperature is monitored using a commercial optical pyrometer; the temperature variation across the central part of the wafer is estimated to be 3 °C. The MBE system is a commercial growth chamber with nine sources located with crucible openings at a distance of approximately 23 cm from the substrate. The axis of the chamber (also the substrate normal) is tilted 30° relative to the horizontal so that the substrate faces somewhat downward, and the source ports are arranged such that each source axis is tilted 29° away from the substrate normal. Other features of the MBE system have been described in detail elsewhere.<sup>12</sup>

The buffers were grown to thicknesses of 100 and 500 nm at a rate of 1  $\mu\text{m}/\text{h}$ . The V/III ratio, measured by an ion gauge beam flux monitor, was 20:1. All 100 nm thick buffer layers were grown at 600 °C without pausing. For 500 nm thick buffer layers, three different buffer deposition schemes were studied: (1) "pulsed start" buffers had Ga deposited (with a continuous As overpressure) in cycles of increasing length separated by 10 s pauses for the initial 100 nm of growth, starting with a 1 s Ga cycle, the remaining 400 nm were grown continuously, and all growth was at 600 °C; (2) "continuous" buffers were grown without pausing at 600 °C; and (3) "annealed" buffers were deposited continuously at 600 °C then held at high temperature for an additional time before cooling. Two annealing times and temperatures were tested. For anneal 1, the sample was held 15 min at 600 °C; for anneal 2, the sample was held 30 min at 500 °C. The sample growth conditions are summarized in Table I.

The roughness and topography of the substrates and buffers were measured by AFM. Samples were imaged under ambient conditions with commercial, reflection coated, pyramidal Si tips in tapping mode. The samples were consistently oriented with the major flat to the bottom of the scan, so that,

TABLE I. Summary of the growth conditions for buffer layer samples. All samples were grown at 600 °C and with a continuous start unless a pulsed start is noted.

Sample label	Wafer treatment	Buffer thickness grown (nm)	Other growth conditions
AR-0	As received	0	
AR-100	As received	100	
AR-500	As received	500	
AR-500 R	As received	500	Repeated sample
AR-500 AN1	As received	500	15 min anneal at 600 °C
AR-500 AN2	As received	500	30 min anneal at 500 °C
AR-500 PS	As received	500	Pulsed start
HCl-0	HCl	0	
HCl-100	HCl	100	
PAW-0	PAW-HCl	0	
PAW-100	PAW-HCl	100	
PAW-500	PAW-HCl	500	
PAW-500 R	PAW-HCl	500	Repeated sample

in all the images shown, the  $[01\bar{1}]$  direction points to the top and the  $[0\bar{1}1]$  direction points to the right. For each sample, a set of three scans of different sizes ( $5 \times 5$ ,  $3 \times 3$ , and  $1 \times 1 \mu\text{m}^2$ ) was obtained at a minimum of three locations in the central  $3 \times 3 \text{ cm}^2$  area of the wafer. Images were processed with a linear "flatten" algorithm in which a straight line is subtracted from each scan line so that the average of each line has zero height. The flatten algorithm was required to remove jumps in the background level (typically on the order of 0.05 nm) caused by changes in tip tracking on some scans. The rms roughness values were determined from the full  $5 \times 5 \mu\text{m}^2$  scans by use of the equation  $R_q = [\sum (z_i - z_{av})^2 / n]^{1/2}$ , where  $z_i$  is the height of each pixel and  $n$  is the number of pixels. Reported roughness values are the average of at least two and, typically, three scans. For comparison to other literature values, the average roughness was also calculated by the equation  $R_a = [(\sum |z_i - z_{av}|) / n]$ .

For all  $5 \times 5 \mu\text{m}^2$  scans, the distribution of pixel heights was also calculated. In this histogram or bearing analysis, all pixels with heights within a 0.015 nm range were binned together. All  $5 \times 5 \mu\text{m}^2$  scans from a sample were combined for this analysis. The result is reported as the bearing percentage, or the percentage of all pixels in the images that fall within each bin.

To analyze the changes in surface topography at different length scales, a tile size analysis similar to that described by Kiely and Bonnell<sup>13</sup> was performed. This analysis highlights the presence of any characteristic length scales in the image, since there will tend to be a change of slope in the graph of roughness versus length scale at the characteristic length. Each image of  $512 \times 512$  pixels was divided into a series of subsets, or tiles, and the rms roughness  $R_q$  was calculated for each set of tiles. For the smallest tile size ( $5 \times 5$  pixels) used, there are  $508 \times 508$  tiles, each of which overlaps its neighbors by all but one row or column of pixels. The rms

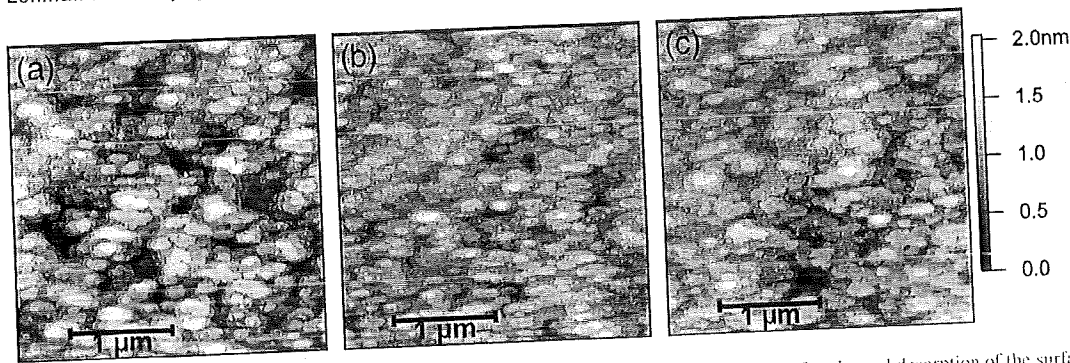


Fig. 3. AFM images of samples after growth of a 100 nm buffer layer. Typical  $3 \times 3 \mu\text{m}^2$  images of samples after thermal desorption of the surface oxide and 100 nm buffer layer growth for wafers which were used (a) as received (AR-100), (b) after HCl treatment (HCl-100), and (c) after PAW-HCl treatment (PAW-100). The z scale for each image is 2 nm.

Further growth of GaAs for a 500 nm thick buffer layer increased the smoothness and left no visible pits on the surface. Typical AFM images of the as-received and PAW-HCl treated wafers after 500 nm GaAs are shown in Figs. 4(a) and 4(b). The quality of the two buffer layers is visually quite similar; the surfaces appear patchy with completely filled oblong terraces several hundred nanometers across. These 500 nm buffer layer growths were repeated for the as-received and PAW-HCl treated wafers to check reproducibility. The rms roughness calculations as a function of sample length scale are shown for these four samples in Fig. 5. While there is a variation of nearly 20% in the calculated roughness  $R_q$  for repeated samples, all the samples

are extremely smooth. Specifically, the calculated rms roughness of the as-received and PAW-HCl treated samples (summarized in Table II) shows no difference in surface smoothness resulting from the pretreatment of the wafer. As in the 100 nm thick buffer layer samples, the characteristic length scale is difficult to define precisely but is approximately 200–400 nm.

#### A. Effects of pre- and postgrowth conditions

As discussed above, the growth conditions for sample AR-500 produce smooth surfaces that appear somewhat patchy, with oblong, completely filled terraces visible in the

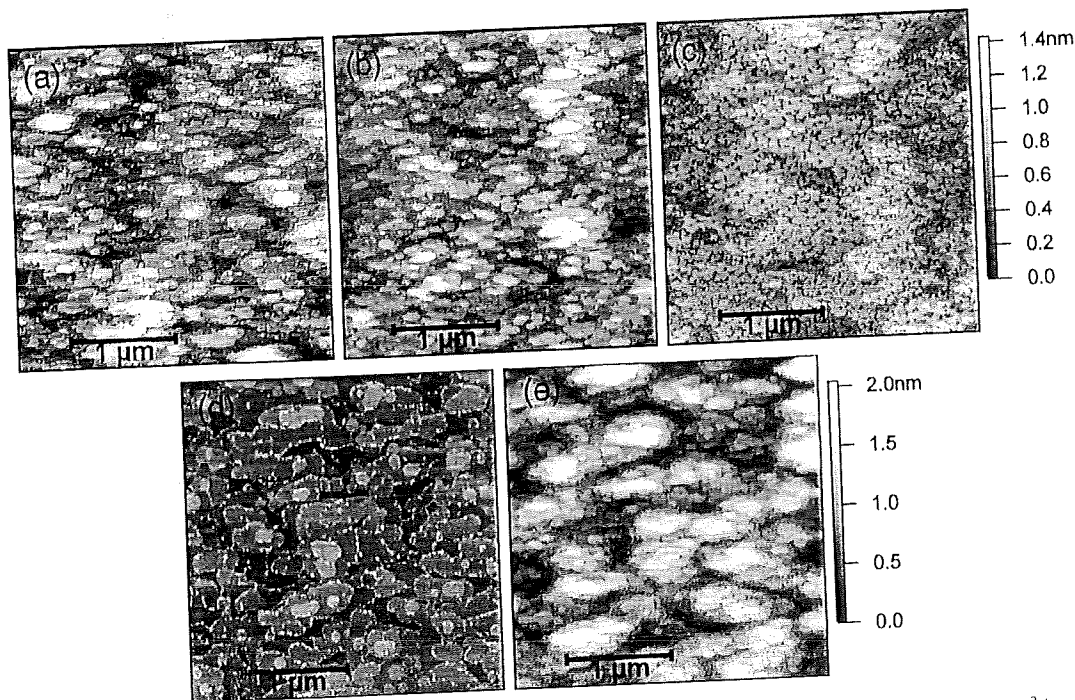


Fig. 4. AFM images of samples after growth of a 500 nm buffer layer with varying pre- and postgrowth conditions. Typical  $3 \times 3 \mu\text{m}^2$  images of samples after thermal desorption of the surface oxide and 500 nm buffer layer growth for wafers (a) as received (AR-500), and (b) after PAW-HCl treatment (PAW-500). The wafers shown in (c)–(e) were all used as received. A 15 min anneal at the growth temperature of 600 °C (anneal 1) produced an extremely smooth surface (c). A longer 30 min anneal at 500 °C (anneal 2) produced a surface (d) that was patchier and less smooth than the high-temperature anneal. A pulsed start of the growth with no anneal resulted in (e) a mounded surface. Note that the z scale for (a)–(c) is 1.4 nm but increases to 2.0 nm for (d) and (e).

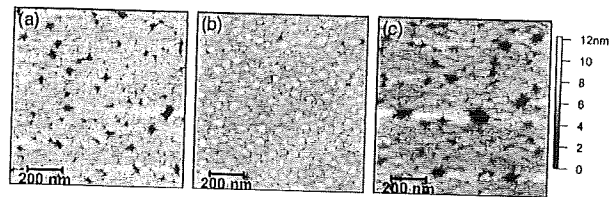


FIG. 1. AFM images of deoxidized samples AR-0, HCl-0, and PAW-0. Typical  $1 \times 1 \mu\text{m}^2$  images of samples after thermal desorption of the surface oxide with no subsequent buffer layer growth for wafers which were used (a) as received, (b) after HCl treatment, and (c) after PAW-HCl treatment. The z scale for each image is 12 nm.

roughness  $R_q$  was calculated for each tile; the mean of all  $R_q$  values calculated for the tile size is reported as the roughness for the length corresponding to the edge length of the tile. The edge length of the tile was incremented by 5 pixels and the mean rms roughness was calculated for each new tile size until the maximum tile size of  $510 \times 510$  was reached. For tiles of  $25 \times 25$  pixels and larger, the amount of overlap between sequential tiles was set to 95% to reduce redundant calculations. For tiles approximately one-quarter of the full image size and larger, the amount of overlap was increased in order to maintain a minimum number of tiles in the calculations. For each sample, the tile size results for all scans of the same size (at least two but typically three scans) were averaged and the standard deviation was calculated. The results from the  $1 \times 1 \mu\text{m}^2$  scans were used for length scales less than 100 nm, and results from the  $5 \times 5 \mu\text{m}^2$  scans were used at all longer length scales.

### III. RESULTS

After the thermal desorption of the surface oxide and without subsequent buffer growth, all samples displayed rough surfaces, as shown by the AFM images in Fig. 1. The wafer pretreated with PAW-HCl (PAW-0) was rougher than

the as-received epi-ready wafer (AR-0), but both contain deep pits and a generally rough surface. The GaAs wafer dipped in HCl (HCl-0) had few, if any, pits and was significantly smoother overall. The rms roughness  $R_q$  as a function of length scale for these samples is shown in Fig. 2. The rms roughness increases steeply as the tile size increases then levels off, indicating a short characteristic length scale of approximately 80–100 nm for these samples. The HCl-0 sample has the sharpest knee in  $R_q$  (around 70 nm), indicating a consistent length scale on the surface that correlates with the white spots visible in the AFM image in Fig. 1(b). Samples AR-0 and PAW-0 show more gradual transitions to the final plateau roughness  $R_q$  due to the variation in size (from 50 to 150 nm width) of the pits in these surfaces.

After only 100 nm growth of GaAs, the surfaces were much smoother regardless of the type of wafer pretreatment. Representative AFM images of the 100 nm buffer layers are shown in Fig. 3. The surfaces appear visually much smoother than the deoxidized samples in Fig. 1 (note the differences in the gray scales and image sizes between those of Figs. 1 and 3), although some irregularities and small pits are still present. As shown in Fig. 2, the rms roughness of the PAW-HCl treated sample PAW-100 is still greater than that of the HCl sample (HCl-100), but the difference is minor, less than 0.03 nm. Although the as-received sample AR-100 is rougher than either PAW-100 or HCl-100, the AR-100 sample was grown significantly later than the other two, so the increase in roughness likely represents sample-to-sample variation due to small changes in the growth environment. For all of these samples the rms roughness increases more slowly with tile size than for the deoxidized samples. The characteristic length scale is difficult to define precisely because the transition to the plateau region is gradual, but it appears to be between 200 and 300 nm, correlating with the sizes of the terraces visible in the AFM images.

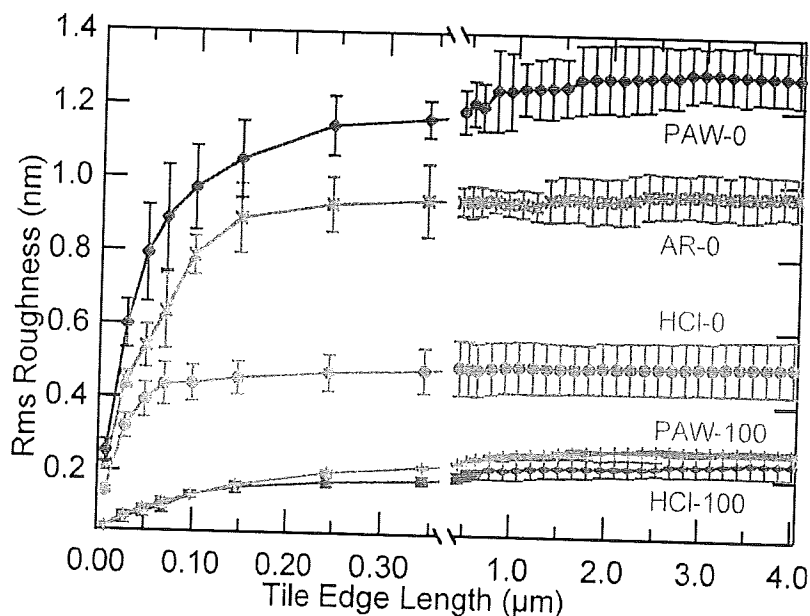


FIG. 2. (Color online) Roughness of deoxidized and 100 nm thick buffer samples. The axis has been expanded for small tile edge lengths. All three deoxidized samples are considerably rougher than any of the grown buffer layer samples. The roughness also increases to its plateau value very quickly in the deoxidized samples, indicating that the characteristic length scale of the roughness is shorter than in the grown buffer samples. The error bars indicate the standard deviation of the roughness values at each tile size.

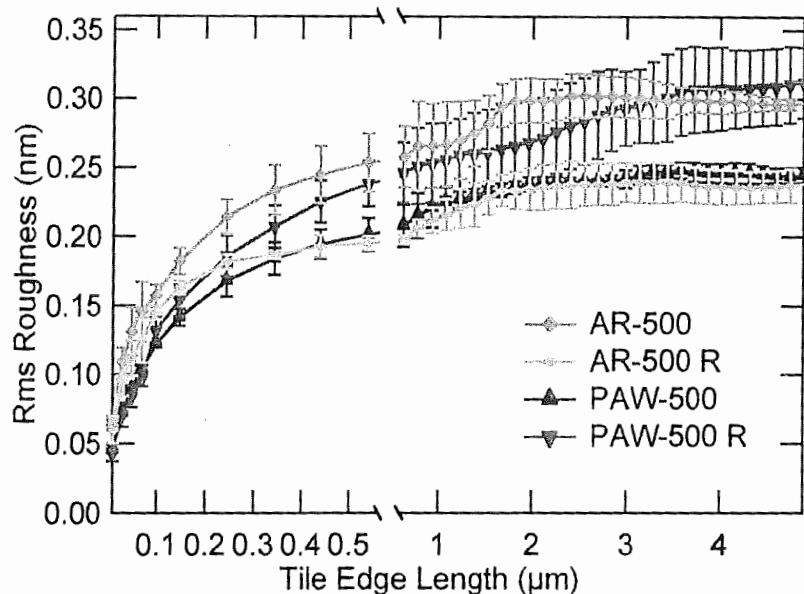


FIG. 5. (Color online) Roughness comparison of samples with 500 nm growth on as-received and PAW treated samples. To check sample-to-sample variation, two samples of 500 nm thickness were grown for both the as-received and the PAW treated wafers. The rms roughness  $R_q$  varies by 15%–20% for both the repeated AR-500 and PAW-500 samples. The samples grown on as-received wafers are as smooth as the samples grown on wafers pretreated with the PAW-HCl treatment before growth, so no sample improvement results from pretreatment.

AFM images [Fig. 4(a)]. Several variations on these growth conditions were tested for their effect on the smoothness and topography of the buffer layers. Sample AR-500 AN1 was annealed for 15 min at the growth temperature of 600 °C. An AFM image of this sample, shown in Fig. 4(c), displays a topography very different from that of the unannealed sample; after the anneal, the surface is covered by very large but incompletely filled terraces. An anneal at lower temperature (anneal 2: 30 min at 500 °C) also produced terraces larger than those observed on unannealed samples. An AFM image of AR-500 AN2 is shown in Fig. 4(d). Although the terraces after the low-temperature anneal are large, they are completely filled, and small islands have developed at the edges of these terraces. We have previously observed<sup>11</sup> similar decorations at terrace edges in a GaAs sample annealed at 530 °C for 5 min, and we speculate that their formation is caused by an increased effect of the step

edge barrier at these lower annealing temperatures. Both the high and low-temperature anneals produce smooth surfaces ( $R_q < 0.28$  nm), as shown by the rms roughness calculations in Fig. 6.

A sample in which the buffer layer was initially grown in pulses developed large mounds on the surface, as shown in Fig. 4(c). In this pulsed growth mode, the supply of Ga was interrupted for brief periods at the start of growth. This technique is not related to migration enhanced epitaxy<sup>7,14,15</sup> in which Ga is supplied to the surface in the absence of As; rather it is similar to the growth interruption technique developed by Sakaki *et al.*<sup>6</sup> to produce flat interfaces for the growth of GaAs/AlAs quantum wells. The mounds observed here are elongated along the  $[01\bar{1}]$  direction and are similar to those previously reported in the literature,<sup>10,11,16–21</sup> although these appear more rounded and less aligned than

TABLE II. Comparison of rms and average roughness for 500 nm buffer layer samples. The rms roughness  $R_q$  and average roughness  $R_a$  were calculated only from full  $5 \times 5 \mu\text{m}^2$  scans.

Sample description	RMS roughness $R_q$ (nm)	Average roughness $R_a$ (nm)
As received, continuous start (AR-500)	$0.298 \pm 0.003$	$0.236 \pm 0.004$
As received, continuous start (AR-500 R)	$0.241 \pm 0.015$	$0.192 \pm 0.013$
AR-500 and AR-500 R combined	$0.27 \pm 0.03$	$0.21 \pm 0.03$
PAW etch, continuous start (PAW-500)	$0.246 \pm 0.006$	$0.197 \pm 0.006$
PAW etch, continuous start (PAW-500 R)	$0.314 \pm 0.024$	$0.249 \pm 0.019$
PAW-500 and PAW-500 R combined	$0.28 \pm 0.04$	$0.22 \pm 0.03$
As received, 15 min anneal at 600 °C (AR-500 AN1)	$0.218 \pm 0.009$	$0.171 \pm 0.003$
As received, 30 min anneal at 500 °C (AR-500 AN2)	$0.267 \pm 0.006$	$0.211 \pm 0.005$
As received, pulsed start (AR-500 PS)	$0.51 \pm 0.03$	$0.39 \pm 0.05$
Results from Allwood <i>et al.</i> <sup>8</sup> 1000 nm buffer layers grown by growth A		
Sample grown 1 week after APM etch	...	0.2
Sample grown at 12 weeks after APM etch	...	4.0
Sample grown at 12 weeks on untreated epi-ready wafer	...	5.4

<sup>8</sup>References 22 and 23.

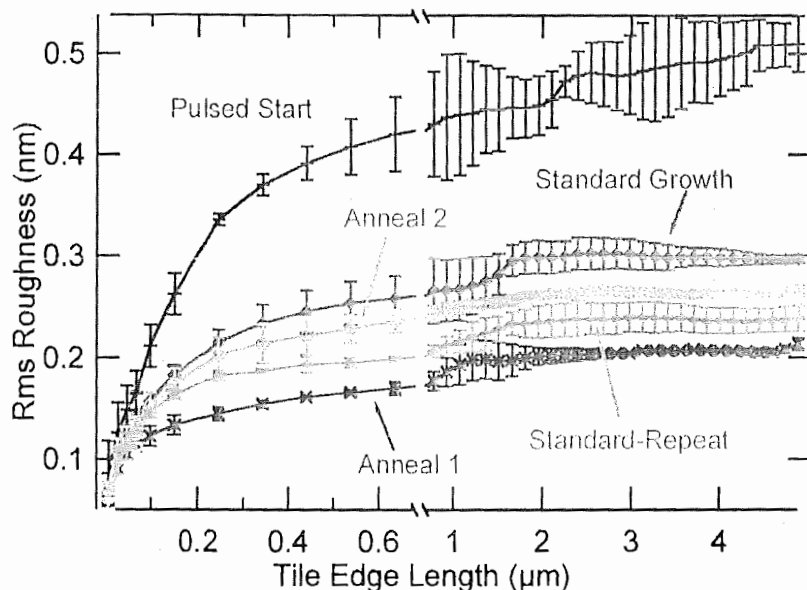


Fig. 6. (Color online) Roughness comparison of different growth conditions for 500 nm growth on as-received samples. The sample AR-500 AN1, which was annealed at the growth temperature of 600 °C for 15 min after material deposition was complete, has the smoothest surface. Sample AR-500 PS, grown using a pulsed start, is considerably rougher than all other samples due to the large mounds that developed during growth. The measured surface roughness varies significantly depending on whether the top or the edge of a mound is being measured; this natural spread in the values results in the larger error bars for this sample.

some of the previously reported mounds. The rms roughness of this pulsed start sample is roughly double that of the continuous start samples, as can be seen from the graph of rms roughness versus length scale shown in Fig. 6. As for the other samples shown, the rms roughness for the pulsed start sample has a gradual transition from the initial step increase to a slowly increasing roughness at longer length scales, indicating that no sharply defined characteristic length scale is present. The transition to the slowly increasing region occurs at approximately 500–700 nm, correlating with the size of the mounds. A well-defined plateau was not observed for this sample within the 5  $\mu\text{m}$  length scale investigated.

## B. Bearing analysis

The variation in height of each sample was also studied by a bearing analysis. In this technique, a histogram of the heights of all pixels in the image is created, providing another way of quantifying the variations in height of the surface. A perfectly flat sample would appear as a sharp delta-function-like peak in the bearing analysis, since all pixels would have the same height; surfaces with more varied features at a range of heights will appear as broader peaks. The bearing analyses for the pulsed start 500 nm buffer, continuous start 500 nm buffer, 600 °C annealed buffer, and 500 °C

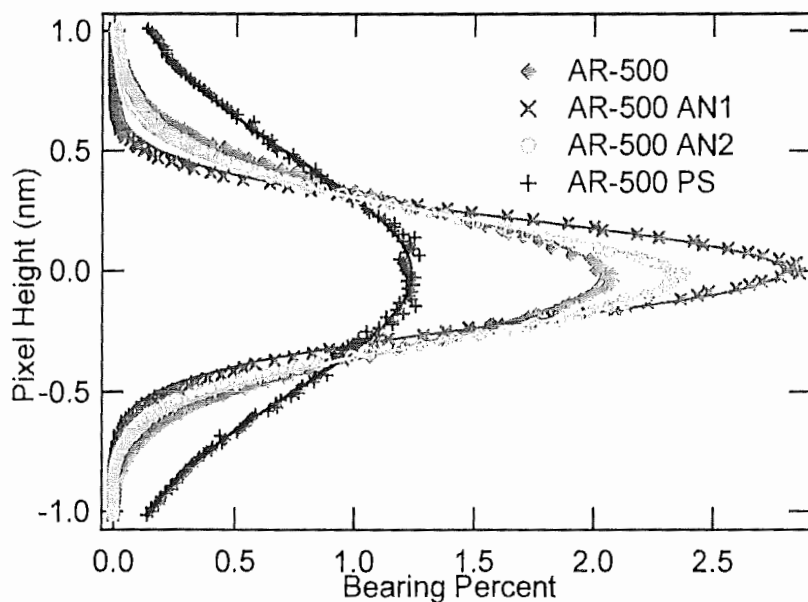


Fig. 7. (Color online) Bearing analysis of different growth conditions for 500 nm buffer layers. The bearing percentage is the percentage of all pixels in the analyzed images that fall within the given height range. Compared to the standard continuous start sample, the pulsed start sample is rough and mounded; this broader range of heights is seen in the bearing analysis as a wider, shorter peak in the distribution of pixel heights. The bearing analysis for the extremely flat annealed sample shows a sharp peak with nearly all the imaged surface within a 1.0 nm range. The pixel height histogram results were fitted to a Gaussian distribution, which is shown as a solid line for each sample.

TABLE III. Gaussian widths, amplitudes, and the peak amplitude to width ratio calculated from the bearing analysis for the 5  $\mu\text{m}$  images of each of the samples. The uncertainty of the Gaussian fit for each sample was 1% of the reported value or less in each case, which is smaller than the sample-to-sample variation. Samples AR-500 and PAW-500 were both repeated, so two values are reported for each. Note that, because of the deep pits present on samples AR-0 and PAW-0, the distributions of pixel heights for those samples were skewed negatively and were not well fitted by the Gaussian distribution. Thus the reported width values for these samples (marked below by asterisks) are not easily comparable to the width values for the other samples.

Buffer	AR			HCl			PAW		
	Width (nm)	Amplitude (%)	Amplitude: width ratio	Width (nm)	Amplitude (%)	Amplitude: width ratio	Width (nm)	Amplitude (%)	Amplitude: width ratio
0	0.61*	1.22	2.0	0.63	1.30	2.1	0.96*	0.73	0.8
100	0.49	1.67	3.4	0.32	2.59	8.0	0.38	2.21	5.8
500	0.34	2.49	7.3				0.35	2.41	6.9
500	0.42	2.03	4.9				0.43	1.94	4.5
500 AN1	0.30	2.79	9.2						
500 AN2	0.36	2.30	6.3						
500 PS	0.69	1.24	1.8						

annealed buffer are shown in Fig. 7. As expected, the mounded sample AR-500 PS has a broader range of pixel heights, so that the peak of the height distribution is both broader and shorter than for the flatter continuous start sample. The smooth annealed sample AR-500 AN1 has an extremely narrow pixel height distribution; nearly all pixels on the surface fall within a 1 nm range. The sample annealed at lower temperature AR-500 AN2 is also extremely smooth but has a slightly broader distribution than the AN1 sample. The distribution of heights was well fitted by a Gaussian distribution for all samples except the rough, pitted, deoxidized samples AR-0 and PAW-0. The peak height and width values (defined from the peak center to the point where the amplitude has decreased by  $1/e$ ) found from these Gaussian fits are shown in Table III. The ratio of the peak amplitude to width is also calculated and serves as an alternative assessment of the surface roughness. The ratio is like a  $Q$  factor for the pixel distribution, so that a higher value for the ratio indicates a smoother, flatter surface. These results show that the bearing analysis provides a good quantitative measure of surface roughness for MBE buffer layers. In particular, the ratio of the height to width of the bearing analysis profile provides a single number that can be used to help distinguish between surfaces with similar roughness values.

#### IV. DISCUSSION

Our finding that, even for aged wafers, chemical pretreatment did not significantly affect surface roughness after growth contrasts with the results of Allwood *et al.*,<sup>22,23</sup> who studied the surface smoothness of GaAs grown by OMVPE. Allwood *et al.* found deterioration of GaAs buffer layer quality for all wafers more than 12 weeks old, but the wafers treated with an ammonia peroxide mixture (APM) etch (2:1:40 solution of  $\text{NH}_4\text{OH}:\text{H}_2\text{O}_2:\text{H}_2\text{O}$ ) before aging had smoother surfaces and fewer visible defects than the as-received epi-ready wafers. Comparing our results, as shown in Table I, we find that, regardless of wafer age or pretreatment, the 500 nm buffer layers grown in this work are as

smooth as the 1000 nm grown on fresh wafers by OMVPE. Even without any buffer layer growth, the surfaces of our roughest substrates are still substantially smoother than the 1000 nm buffer layers grown on aged substrates by OMVPE. The differences suggest that oxide desorption and buffer layer smoothness in the MBE growth environment are less sensitive to substrate aging and pretreatment than for the OMVPE growth environment.

Several methods of minimizing pitting of the surface during oxide removal have been proposed in the literature, including the deposition of Ga well below the growth temperature in the absence of an As flux<sup>24–26</sup> and treatment with atomic hydrogen (AH).<sup>4,27–29</sup> Khatiri *et al.*<sup>28</sup> reported a rms roughness of  $0.18 \pm 0.01$  nm (calculated from a  $200 \times 200$  nm<sup>2</sup> STM scan) for (100) GaAs after exposure to AH. After annealing under  $\text{As}_2$  and growth of a thin 100 ML (monolayer) buffer layer, the rms roughness drops to as low as  $0.11 \pm 0.01$  nm. These samples appear extremely smooth, although it is difficult to compare the rms roughness values directly to our results since the images of Khatiri *et al.* are at a smaller length scale and are acquired by STM rather than AFM. Using the Ga-deposition technique, Asaoka<sup>24</sup> reported a minimum rms roughness of 0.16 nm (calculated from AFM scans of unspecified size) after oxide removal.

Mounds<sup>10,11,16–21</sup> or undulations<sup>30</sup> elongated along the  $[01\bar{1}]$  direction have been widely observed during GaAs homoepitaxy although the size and shape of the mounds vary widely in the AFM images available in the literature. The mounds have often been attributed to an unstable growth mode<sup>16,17,20</sup> due to the Schwoebel barrier at the step edge.<sup>31,32</sup> In this model, mounding should be observed when growth conditions act to increase adatom diffusivity, consequently increasing the effect of the step edge barrier. An alternate explanation for mound formation has been proposed by Ballestad *et al.*<sup>33,34</sup> Instead of attributing the mounds to a growth instability, they modeled the surface using the anisotropic Kardar–Parisi–Zhang equation<sup>35</sup> and found that the mound formation could be accounted for simply by a rough starting surface.

In the sample grown for this work, it is clear that the formation of the surface mounds is related to the initial growth conditions rather than to the roughness of the starting surface, as proposed by Ballestad *et al.*,<sup>33,34</sup> since the mound formation can be controlled simply by changing from a continuous to a pulsed growth. These results are consistent with the model in which the Schwoebel barrier promotes mound formation. When the growth is pulsed, the growth pauses allow Ga adatoms to travel farther on the surface before sticking to a site. The enhanced diffusivity increases the effect of the Schwoebel barrier by making it more likely for the adatom to encounter the step edge. This explanation is also consistent with the results of Lengel *et al.*, who observed mounding on GaAs samples grown with V/III ratios of 4:1 and below.<sup>19</sup> Because less As is available for bonding, the Ga diffusion distance is longer for lower V/III ratios. By increasing the V/III ratio to between 8:1 and 11:1, Lengel *et al.* obtained smooth layers of GaAs.<sup>19</sup> This is consistent with our results: our samples are grown with a V/III ratio of 20:1 and have a smooth, layered morphology, except in the situation of the pulsed start.

## V. SUMMARY

The roughness of homoepitaxial GaAs buffer layers grown by MBE was studied by a quantitative analysis of multiple, large-area AFM images. The variation in roughness with length scale was found by using a tiling analysis in order to determine the characteristic length scales present in the surface topography. The buffer layers were also characterized by a bearing analysis as an alternative method of quantifying the surface smoothness. Although the etching pretreatments caused significantly different starting surfaces after the oxide desorption, after only 100 nm of buffer layer growth all samples were very similar in AFM imaging and fairly smooth, with a rms roughness ranging from 0.27 to 0.40 nm. After 500 nm buffer layer growth, samples were very smooth ( $R_q \approx 0.27$  nm) and indistinguishable, showing no significant effects from the wafer pretreatment, even for aged wafers. In this case, storing epi-ready GaAs wafers in their original packaging in ambient conditions for more than 1 year has been shown not to adversely affect the quality of MBE growth on those wafers. Annealing the sample by holding it for 15 min at the growth temperature of 600 °C after buffer growth improved the surface roughness, reducing it to  $0.218 \pm 0.009$  nm. Beginning the buffer layer growth with short pulses of Ga as the wafer cooled from 640 to 600 °C was shown to cause mounding on the surface of the wafer. In this case, surface mounding appears related to growth conditions rather than the pregrowth surface roughness of the substrate.

- <sup>1</sup>G. R. Bell, T. S. Jones, J. H. Neave, and B. A. Joyce, *Surf. Sci.* **458**, 247 (2000).
- <sup>2</sup>T. Hashizume, Q. K. Xue, J. Zhou, A. Ichimiya, and T. Sakurai, *Phys. Rev. Lett.* **73**, 2208 (1994).
- <sup>3</sup>T. Ide, A. Yamashita, and T. Mizutani, *Phys. Rev. B* **46**, 1905 (1992).
- <sup>4</sup>A. Khatiri, J. M. Ripalda, T. J. Krzyzewski, G. R. Bell, C. F. McConville, and T. S. Jones, *Surf. Sci.* **548**, L1 (2004).
- <sup>5</sup>N. Ikarashi, M. Tanaka, H. Sakaki, and K. Ishida, *Appl. Phys. Lett.* **60**, 1360 (1992).
- <sup>6</sup>H. Sakaki, M. Tanaka, and J. Yoshino, *Jpn. J. Appl. Phys., Part 2* **24**, L417 (1985).
- <sup>7</sup>E. Briones and Y. Horikoshi, *Jpn. J. Appl. Phys., Part 1* **29**, 1014 (1990).
- <sup>8</sup>S. Ritchie, S. R. Johnson, C. Lavoie, J. A. Mackenzie, T. Tiedje, and R. Streeter, *Surf. Sci.* **374**, 418 (1997).
- <sup>9</sup>G. W. Smith, A. J. Pidduck, C. R. Whitehouse, J. L. Gasper, A. M. Keir, and C. Pickering, *Appl. Phys. Lett.* **59**, 3282 (1991).
- <sup>10</sup>G. W. Smith, A. J. Pidduck, C. R. Whitehouse, J. L. Gasper, and J. Spowart, *J. Cryst. Growth* **127**, 966 (1993).
- <sup>11</sup>A. Roshko, T. E. Harvey, S. Y. Lehman, R. P. Mirin, K. A. Bertness, and B. L. Hyland, *J. Vac. Sci. Technol. B* **23**, 1226 (2005).
- <sup>12</sup>T. E. Harvey, K. A. Bertness, R. K. Hiecknell, C. M. Wang, and J. D. Splett, *J. Cryst. Growth* **251**, 73 (2003).
- <sup>13</sup>J. D. Kiely and D. A. Bonnelli, *J. Vac. Sci. Technol. B* **15**, 1483 (1997).
- <sup>14</sup>Y. Horikoshi and M. Kawashima, *J. Cryst. Growth* **95**, 17 (1989).
- <sup>15</sup>Y. Horikoshi, M. Kawashima, and H. Yamaguchi, *Jpn. J. Appl. Phys., Part 1* **27**, 169 (1988).
- <sup>16</sup>M. D. Johnson, C. Orme, A. W. Hunt, D. Graff, J. Sudijono, L. M. Sander, and B. G. Orr, *Phys. Rev. Lett.* **72**, 116 (1994).
- <sup>17</sup>C. Orme, M. D. Johnson, J. L. Sudijono, K. T. Leung, and B. G. Orr, *Appl. Phys. Lett.* **64**, 860 (1994).
- <sup>18</sup>C. Orme, M. D. Johnson, K. T. Leung, and B. G. Orr, *Mater. Sci. Eng., B* **30**, 143 (1995).
- <sup>19</sup>G. Lengel, R. J. Phaneuf, E. D. Williams, S. Das Sarma, W. Beard, and F. G. Johnson, *Phys. Rev. B* **60**, RS469 (1999).
- <sup>20</sup>G. Apostolopoulos, J. Herfort, L. Daweritz, K. H. Ploog, and M. Luysberg, *Phys. Rev. Lett.* **84**, 3358 (2000).
- <sup>21</sup>W. Ye, S. Hanson, M. Reason, X. Weng, and R. S. Goldman, *J. Vac. Sci. Technol. B* **23**, 1736 (2005).
- <sup>22</sup>D. Allwood, N. Mason, A. Mowbray, and R. Palmer, *J. Cryst. Growth* **248**, 108 (2003).
- <sup>23</sup>D. A. Allwood, S. Cox, N. J. Mason, R. Palmer, R. Young, and P. J. Walker, *Thin Solid Films* **412**, 76 (2002).
- <sup>24</sup>Y. Asaoka, *J. Cryst. Growth* **251**, 40 (2003).
- <sup>25</sup>J. H. Lee, Z. M. Wang, and G. J. Salamo, *Appl. Phys. Lett.* **88**, 252108 (2006).
- <sup>26</sup>Z. R. Wasilewski, J. M. Baribeau, M. Beaulieu, X. Wu, and G. I. Sproule, *J. Vac. Sci. Technol. B* **22**, 1534 (2004).
- <sup>27</sup>K. G. Byink and L. Grazulis, *J. Vac. Sci. Technol. B* **23**, 554 (2005).
- <sup>28</sup>A. Khatiri, T. J. Krzyzewski, C. F. McConville, and T. S. Jones, *J. Cryst. Growth* **282**, 1 (2005).
- <sup>29</sup>P. Tomkiewicz, A. Winkler, and J. Szuber, *Appl. Surf. Sci.* **252**, 7647 (2006).
- <sup>30</sup>K. Ikuta, J. Osaka, and H. Yokoyama, *J. Cryst. Growth* **136**, 114 (1994).
- <sup>31</sup>R. L. Schwoebel and E. J. Shipsey, *J. Appl. Phys.* **37**, 3682 (1966).
- <sup>32</sup>J. Villain, *J. Phys. I* **1**, 19 (1991).
- <sup>33</sup>A. Ballestad, B. J. Ruck, M. Zdamecyk, T. Pinnington, and T. Tiedje, *Phys. Rev. Lett.* **86**, 2377 (2001).
- <sup>34</sup>A. Ballestad, B. J. Ruck, J. H. Schmid, M. Adamecyk, E. Nodwell, C. Nicoll, and T. Tiedje, *Phys. Rev. B* **65**, 205302 (2002).
- <sup>35</sup>A. Pimpinelli and J. Villain, *Physics of Crystal Growth* (Cambridge University Press, Cambridge, 1998).